Heterojunctions Based on II-VI Compound Semiconductor One-Dimensional Nanostructures and Their Optoelectronic Applications

Xiwei Zhang [1],*, **Di Wu [2]** and **Huijuan Geng [1]**

[1]   College of Physics and Electrical Engineering, Anyang Normal University, Anyang 455000, China; apnano@outlook.com
[2]   Department of Physics and Engineering, and Key Laboratory of Material Physics, Zhengzhou University, Zhengzhou 450000, China; ciwee@126.com
*   Correspondence: xwezhang@outlook.com; Tel.: +86-372-2900041

Abstract: Wide band gap II-VI semiconductor nanostructures have been extensively studied according to their great potentials for optoelectronic applications, while heterojunctions are fundamental elements for modern electronic and optoelectronic devices. Subsequently, a great deal of achievements in construction and optoelectronic applications of heterojunctions based on II-VI compound semiconductor one-dimensional nanostructures have been obtained in the past decade. Herein, we present a review of a series of progress in this field. First, construction strategies towards different types of heterojunctions are reviewed, including core-shell heterojunctions, one-dimensional axial heterojunctions, crossed nanowires heterojunctions, and one-dimensional nanostructure/thin film or Si substrate heterojunctions. Secondly, optoelectronic applications of these constructed heterojunctions, such as photodetectors, solar cells, light emitting diodes, junction field effect transistors, etc., are discussed briefly. This review shows that heterojunctions based on II-VI compound semiconductor 1-D nanostructures have great potential for future optoelectronic applications.

Keywords: heterojunctions; II-VI semiconductor; one-dimensional nanostructures; optoelectronic applications

1. Introduction

One-dimensional (1-D) semiconductor nanostructures have been attracting a great deal of attention due to their excellent electronic and optoelectronic performance [1–5]. Many high efficiency device applications were achieved based on building blocks of semiconductor nanostructures, such as photodetectors, solar cells, laser diodes, field-effect transistors, etc. [6–9]. On the other hand, wide band gap II-VI semiconductors have been extensively studied for many years according to their great potentials for optoelectronic applications: blue-green laser diodes based on ZnSe [10], high-efficiency solar cells based on CdTe thin films [11], high performance radiation detecting devices based on CdZnTe [12], etc. However, there are still many difficulties in synthesis high quality II-VI semiconductor films, which hindered their electronic and optoelectronic applications. Low-dimensional, particularly one-dimensional II-VI semiconductors, have many advantages over film/bulk counterparts, such as high crystalline perfection, reduced defects and controlled doping, etc. [13]. Furthermore, they also presented excellent properties arising from unique geometries and size-confinement effects [14]. For instance, a CdS/CdSe/CdS biaxial nanobelt with well-defined morphology was synthesized for high sensitivity and excellent stability photodetector, which had superior performance than thin film/bulk configurations due to its high crystal and large surface-to-volume ratio [15].

Heterojunctions are fundamental elements for modern electronic and optoelectronic devices [16,17]. With the rapid development of nanotechnology, heterojunctions based on semiconductor nanostructures have caught the eye of investigators all over the world due to their excellent properties. Different types of nanoscale heterojunction, such as axial, core-shell, and crossed heteorjunctions, have been constructed based on GaN, Si, ZnO, etc. [18–20]. It should be pointed out that the nanoscale heterojunctions have superior performances in terms of atomically sharp interfaces, fewer interface defects, and higher emitting efficiency compared to their thin film and bulk counterparts. As a result, they open up promising future for high-performance device applications, such as light emitting diodes, laser diodes, photodetectors, and solar cells [21–24]. However, there are still many challenges in heterojunction fabrication process so as to be suitable for large scale and stable device applications.

Herein, we present a review on heterojunctions based on II-VI compound semiconductor one-dimensional nanostructures and their optoelectronic applications. First, construction strategies toward different types of heterojunctions are reviewed, including core-shell heterojunctions, one-dimensional axial heterojunctions, crossed nanowires heterojunctions, and one-dimensional nanostructure/thin film or Si substrate heterojunctions. Secondly, optoelectronic applications of these constructed heterojunctions, such as photodetectors, solar cells, light emitting diodes, junction field effect transistors, etc., are discussed briefly. This review shows that heterojunctions based on II-VI compound semiconductor 1-D nanostructures have great potential for future optoelectronic applications.

2. Construction Strategies of Heterojunctions Based on II-VI Compound Semiconductor 1-D Nanostructures

2.1. Core-Shell Heterojunctions

Core-shell heterojunctions based on one-dimensional semiconductor nanostructures exhibit unique advantages in terms of increased surface, shortened carrier collection path, and reduced reflection, which are vitally important for high-performance electronic and optoelectronic nano-devices. On the other hand, core-shell heterojuntions have been of particular interest in that their properties can be easily tuned by changing the diameter and the chemical composition of both the core and the shell. Heretofore, a number of strategies have been developed to construct core-shell heterojunctions, including chemical vapor deposition (CVD), atomic layer deposition (ALD), pulsed laser deposition (PLD), solution-based cation exchange reaction, sputtering, and molecular beam epitaxy (MBE). For core-shell heterojunctions based on II-VI compound semiconductors, two-steps methods were usually used as construction approaches. Wang et al. reported on the construction of p-n junctions based on crystalline Ga-doped CdS-polycrystalline ZnTe nanostructures [25]. They first used thermal evaporation method to synthesize n-type CdS nanowires on Au film-coated silicon substrates. Ga and Ca_2O_3 were used as n-type dopants. Secondly, the p-type ZnTe shell doped with Sb was deposited on the as-synthesized n-type CdS nanowires through another thermal evaporation process. Transmission electron microscope (TEM) imagery showed that there was a sharp distinction in contrast along the radial direction of the nanowire, which revealed its core-shell structure (Figure 1a). Figure 1b shows a HRTEM image of the CdS-ZnTe core-shell nanowire, which depicted that the CdS core had single crystal structure while the ZnTe shell was composed of a large number of crystal grains with a size of 5–10 nm. Furthermore, the elemental mapping in Figure 1c–g clearly displays the spatial distributions of S, Cd, Te, and Zn in the core and the shell. This showed that the ZnTe shell layer continuously covered the entire surface of the CdS nanowire core. Zhou et al. successfully synthesized nearly lattice matched all wurtzite CdSe/ZnTe core-shell nanowires on silicon substrates [26]. CdSe and ZnTe have a small lattice mismatch and similar thermal expansion coefficients, which is beneficial to construct a high-quality heteroepitaxial junction and could reduce the interfacial recombination originating from the interface defects. Zhou and his co-workers first used a thermal evaporation method to synthesize CdSe nanowires. Then, the ZnTe shell was grown epitaxially over the CdSe core using the core as a growth template in a PLD system. Structural characterizations

depicted that both the CdSe core and the ZnTe shell are single crystalline in a wurtzite structure. Furthermore, the core-shell interface can only be distinguished with the assistance of slightly-distorted lattice fringes due to a small lattice mismatch of 0.08% between wurtzite CdSe and wurtzite ZnTe (Figure 2). That is to say, the CdSe core literally acts as a structural template for the ZnTe shell and the interface between them is high-quality and abrupt. Otherwise, photoluminescence and Raman spectroscopy characterization indicate efficient separation of photo-generated electron-hole pairs across the CdSe/ZnTe interface, which mean that the heterojunction could have high performance in optoelectronics devices. Yang et al. used a low-temperature solution-based cation exchange reaction to create a heteroepitaxial junction between a single-crystalline CdS core and single-crystalline Cu_2S shell [27]. The solution method has a much lower cost and better reproducibility than MBE and CVD methods. They first synthesized CdS nanowires by a physical vapor transport method. Then, the as-grown CdS nanowire was dipped into CuCl solution to convert the surface CdS to a Cu_2S shell. TEM characterization depicted that both CdS and Cu_2S are single crystal as shown in Figure 3. Furthermore, the lattice mismatch of CdS and Cu_2S is less than 4%, allowing epitaxial growth with minimal formation of structural defects. On the other hand, the in situ electron energy loss spectrum (EELS) mapping shows that cadmium is uniformly dispersed throughout the nanowire, whereas copper is concentrated near the surface, confirming the core-shell structure. Zhang et al. fabricated coaxial ZnSe/ZnO nanostructures by coating a ZnO thin film on the surface of pre-synthesized p-type ZnSe 1-D nanostructures by a sputtering method [28]. After the sputtering process, a layer of polycrystalline ZnO nanoparticles is attached to the single crystalline ZnSe one-dimensional nanostructure synthesized by a thermal evaporation method. Owing to the n-type behavior of ZnO resulting from intrinsic defects, the core-shell ZnSe/ZnO heterojunction could act as a p-n junction and play an important role in optoelectronic devices. Jie et al. constructed Ge-CdS core-shell heterojunction nanowires via a facile ALD technique [29]. The ALD method can be easy to precisely control the thickness and component of the shell, which is beneficial to tune the optoelectronic properties of heterojunctions. Jie et al. also produced core-shell ZnSe/Si nanocables by a simple two-step growth method [30]. ZnSe nanowire cores were first synthesized by thermal evaporation and then followed by the CVD growth of Si shells. Structure characterization indicated that the ZnSe core had a cubic single-crystal structure while the Si shell was polycrystalline and composed of a large number of crystal grains. Moreover, the authors achieved p-type doping of Si shell by Boron diffusion and constructed a core-shell structure p-n junction, which is favored for optoelectronic applications. Fang et al. synthesized a kind of heterocrystalline-ZnS/single-crystalline-ZnO biaxial nanobelts and a kind of side-to-side single-crystalline ZnS/ZnO biaxial nanobelts via a simple one-step thermal evaporation method. In the ZnS/ZnO biaxial nanobelts, a ZnS domain is composed on the heterocrystalline superlattice $(3C\text{-}ZnS)_N/(2H\text{-}ZnS)_M[111]\text{-}[0001]$ with the atomically smooth interface between wurtzite and zinc blende ZnS fragments [31,32]. Fang et al. also fabricated $ZnO\text{-}Ga_2O_3$ core-shell microwires by a simple one-step chemical vapor deposition method. The ZnO crystal lattice could abruptly switch to the Ga_2O_3 crystal lattice within 6–8 atomic layers without incurring noticeable structure defects at the interface [33].
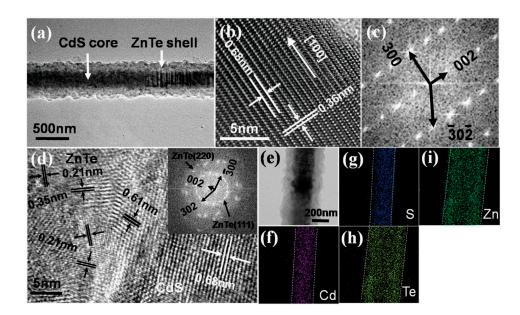
Figure 1. (**a**) TEM image of a CdS-ZnTe core-shell nanowire. (**b**) HRTEM image of the CdS nanowire; and (**c**) the corresponding FFT pattern. (**d**) High-magnification TEM image of a CdS-ZnTe core-shell nanowire. (**e–i**) TEM image of an individual core-shell nanostructure and the corresponding elemental mapping images for: Cd (**f**); S (**g**); Te (**h**); and Zn (**i**). Reproduced with permission from [25], Copyright 2015, The Royal Society of Chemistry.
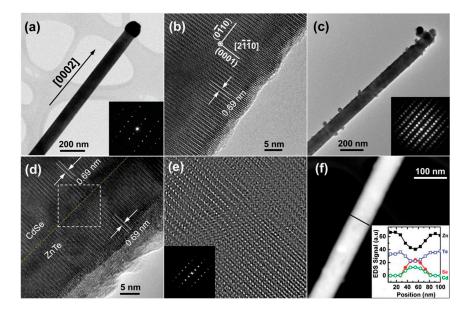

Figure 2. Structural characterization of a CdSe nanowire and CdS/ZnTe core-shell nanowire. (**a**) Low magnification TEM image of an individual CdSe nanowire. Inset: the corresponding SAED pattern. (**b**) HRTEM of a CdSe nanowire demonstrating a single-crystalline, WZ structure. (**c**) A representative TEM image of an individual CdSe/ZnTe core-shell nanowire. Inset: the corresponding CBED pattern. (**d**) HRTEM images of the core-shell interface that display the interplanar spacing and epitaxial growth of the WZ ZnTe shell on the WZ CdSe core. (**e**) Inverse FFT image. Inset: core-shell interface processed from the white, dashed rectangle in (**d**). (**f**) A STEM image of a CdSe/ZnTe core-shell nanowire. Inset: EDS data obtained with a nanoprobe scan along the black line that extends axially across the interface. Reproduced with permission from [26], Copyright 2014, The Royal Society of Chemistry.
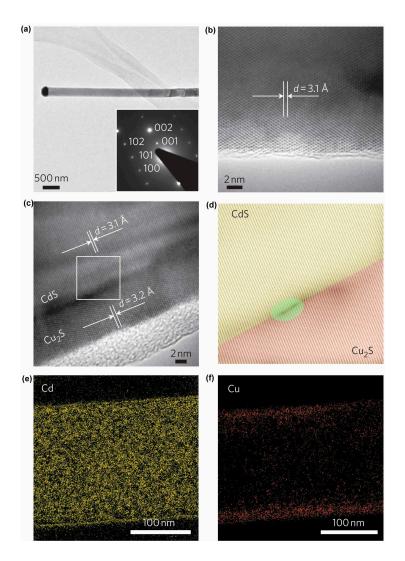
Figure 3. Structural characterization of CdS and CdS-Cu$_2$S core-shell nanowires. (**a**) Representative TEM image of an as-grown CdS nanowire with its tip capped by a gold nanoparticle. Inset: electron diffraction pattern taken on the single crystalline nanowire. (**b**) High-resolution TEM image of an individual CdS nanowire, showing the single crystalline structure. (**c**) High-resolution TEM image of a CdS-Cu$_2$S nanowire at the heterojunction. (**d**) Constructed inverse FFT image along the growth direction for the area marked in c. The green area shows the typical lattice fringe distortion at the core-shell interface (see Supplementary Information). (**e,f**) EELS elemental mapping images for: Cd (**e**); and Cu (**f**). Reproduced with permission from [27], Copyright 2011, Nature Publishing Group.

Regarding the core-shell architecture, 3-D core-shell nanowire array structure provides additional advantages over single nanowire-based devices owing to their unique features, such as a large surface area, excellent multichannel charge transport, and enhanced light absorption through light trapping and scattering. Zhou et al. fabricated a type of CdSe/ZnTe core-shell nanowire array for broad spectral detecting [34]. They first grew vertically aligned CdSe nanowire array on muscovite mica substrate by CVD method. Then, the as-synthesized CdSe nanowire array was transferred to a PLD system for coating ZnTe on CdSe nanowire array. The EDS line scan across the nanowire clearly demonstrated a characteristic core-shell elemental distribution, further confirming the successful synthesis of a CdSe/ZnTe core-shell nanowire array with an abrupt, nearly lattice-matched interface. Wang et al. constructed a fully wide band gap ZnO/ZnS type-II heterojunction core-shell nanowire array for high-performance broad UV/VIS photo-detecting [35]. ZnO nanowire array was first synthesized on ITO substrates and a ZnS shell layer was deposited by the PLD method. A HRTEM

image of a typical single ZnO/ZnS core-shell nanowire shows that two different lattice fringes corresponding to the zinc-blend ZnS shell and wurtzite ZnO core separated by an abrupt interface can be seen (Figure 4). Furthermore, EDS line scan collected along the lateral direction of a core-shell nanowire shows the characteristic core-shell element distribution, which confirms the successful synthesis of ZnO/ZnS core-shell nanowires.
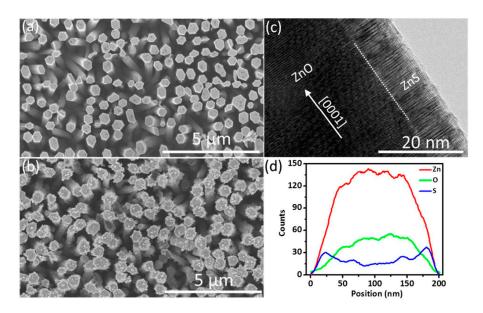

Figure 4. Structural characterization of a ZnO/ZnS core/shell nanowire showing low magnification top view, FESEM images of: (**a**) an as-grown, ZnO nanowire array; and (**b**) a ZnO/ZnS core/shell nanowire array; (**c**) an HRTEM image of a single ZnO/ZnS core/shell nanowire; and (**d**) the corresponding energy dispersive spectroscopy (EDS) lateral line scan depicting elemental peaks characteristic to core/shell nanowire structure. Reproduced with permission from [35], Copyright 2015, American Chemical Society.

2.2. 1-D Axial Heterojunctions

The axial geometry of 1-D axial heterojunction is promising for integrating several p-n junctions in a multi-junction optoelectronic devices, since it offers a large degree of material design freedom due to efficient strain relaxation for lattice mismatched materials [36]. In addition, 1-D axial heterojunction is considered to be fabricated more easily than core-shell approaches and expected to exhibit lower leakage currents and, therefore, should possess a superior rectifying behavior compared to radial structures [37]. 1-D axial heterojunctions, based on II-VI compound semiconductor nanostructures, have also caught the eye of investigators and present excellent performance. For instance, Zhang et al. constructed a kind of p-n heterojunction arrays by directly growing the p-type ZnSe nanoribbons on highly-aligned n-type Si nanowires arrays [38]. Cross-section SEM images showed that quasi-aligned ZnSe nanoribbons array was directly grown on the top of SiNWs array. HRTEM images taken from the junction interface area depict that ZnSe exhibits good epitaxial relationship with the SiNW due to their matched lattice structure (Figure 5). This unique materials combination and structure make it present excellent photovoltaic performance. Furthermore, to overcome the difficulty in complicated multi-step preparation process and high preparation cost, Zhang et al. exploited a facile method to fabricate single ZnSe-ZnO nanowire axial p-n junction by regioselectively oxidizing the p-type ZnSe nanowire in air as shown in Figure 6 [39]. They firstly transferred the as-synthesized p-type ZnSe nanowires onto the SiO_2/Si substrate by a sliding transfer process. After that, Si_3N_4 protection layer was deposited on one end of the ZnSe nanowire via photolithography and magnetron sputtering techniques. Then, the sample was put into rapid thermal process system to oxidize the bare part of ZnSe nanowire at 700 °C in air. The Si_3N_4 layer could protect the covered nanowire part against being

oxidized. As a result, regioselective oxidation of the ZnSe nanowire was achieved. Subsequently, the Si$_3$N$_4$ layer was etched by reactive ion etching and the unoxidized ZnSe part was uncovered. After the regioselective oxidation process, the whole nanowire consists, in part, of unoxidized ZnSe and, in part, of post-oxidized ZnO, which constructed the ZnSe-ZnO axial p-n junction.
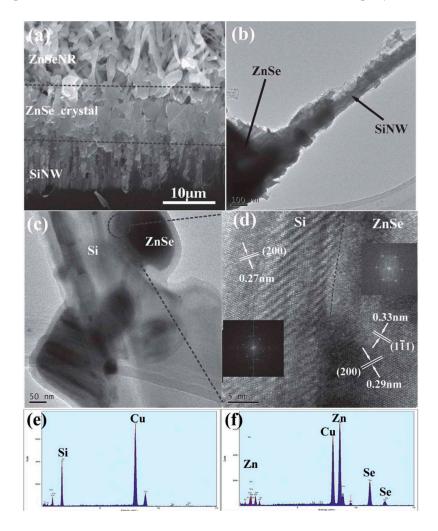

Figure 5. (**a**) Cross-section FESEM image of the ZnSeNR/SiNW heterojunction array. (**b,c**) TEM images of a single SiNW covered by the ZnSe layer. (**d**) HRTEM of the SiNW and ZnSe interface detected at the circle region in (**c**). The junction interface was marked with a dashed line. Insets show the fast Fourier transform (FFT) patterns of the SiNW (left) and ZnSe (right). (**e**) EDX spectrum of the SiNW taken from the light area in (**c**). (**f**) EDX spectrum of the ZnSe taken from the dark area in (**c**). Cu peaks come from the Cu grid used for TEM investigation. Reproduced with permission from [38], Copyright 2011, The Royal Society of Chemistry.
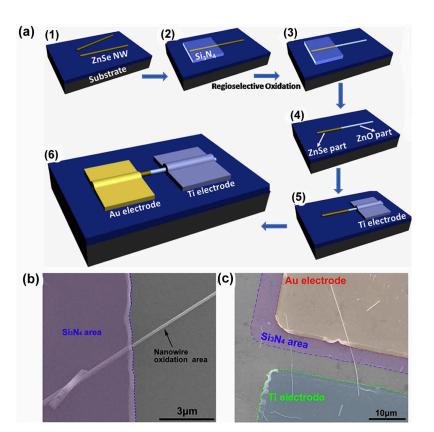
Figure 6. (**a**) Schematic illustration of the construction process of the ZnSe-ZnO axial p-n junction. (**b**) The SEM image of a nanowire whose bare part has already been oxidized. (**c**) The SEM image of a prepared ZnSe-ZnO nanowire axial p-n junction. Reproduced with permission from [39], Copyright 2015, Elsevier B.V.

2.3. Crossed Nanowire Heterojunctions

Core-shell heterojunctions and 1-D axial heterojunctions are always fabricated via a series of complicated multi-step nanostructure preparation process. On the other hand, investigators try to assemble 1-D nanostructures after their synthesis in order to construct heterojunctions. The crossed nanowire heterojunction is a kind of post-assembly heterojunction and presents many advantages, including the ability to: (1) flexibly choose component materials; (2) independently tune the dopant concentration of the component materials; (3) define abrupt, nanoscale junctions that are ideal for high spatial resolution; and (4) assemble arrays for integrated nano-optoelectronic devices [40]. Lieber et al. fabricated crossed n-CdS and p-Si nanowire heterojunctions by microfluidic-directed assembly using orthogonal sequential flows of the CdS and Si nanowires [41]. Furthermore, they constructed a crossed nanowire architecture by sequential deposition of p-type (Si) and n-type (CdS, CdSSe, CdSe, CaN, and InP) nanowire materials using directed fluidic assembly. The crossed nanowire heterostructures are electrically addressable at the cross points and can be described qualitatively by a staggered type-II band diagram heterojunctions [42]. Nie et al. developed another approach to fabricated ZnSe/ZnO crossed heterojunctions (Figure 7) [43]. They firstly dispersed n-type ZnO nanowires on the substrate. Then, p-type ZnSe nanowires were transferred onto the substrate at a vertical direction to the ZnO nanowires by a contact sliding transfer method.
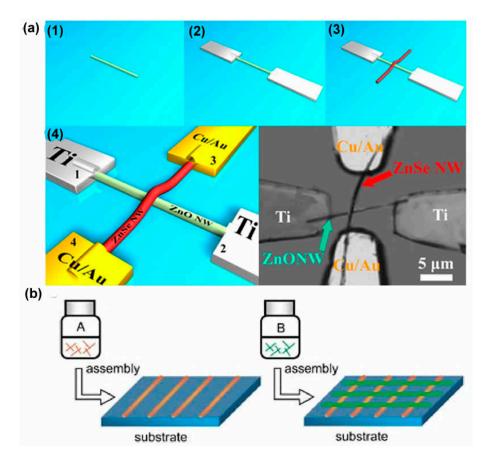
Figure 7. (**a**) Schematic illustration of the step-wise process for the fabrication of a ZnSe nanowire/ZnO nanowire p-n junction and a typical SEM image of the p-n junction device. Reproduced with permission from [43], Copyright 2013, Institute of Physics. (**b**) Schematic of the assembly of crossed nanowire heterojunctions. First, a parallel array of A NWs (orange lines) is aligned on the substrate using a fluidic assembly method, and then a second parallel array of B NWs (green lines) is deposited orthogonally to achieve a crossed NW matrix. Reproduced with permission from [42], Copyright 2005, Wiley-VCH.

2.4. 1-D Nanostructure/Thin Film or Si Substrate Heterojunctions

II-VI group semiconductor one-dimensional nanostructures and Si substrates/semiconductor films could be combined and be used to construct heterojunctions. There are many advantages of this construction strategy: (1) it could avoid the complicated multi-step preparation and simply the procedure of device fabrication; (2) it is compatible with traditional microelectronic technology; and (3) it is suitable to develop align plane array integrated devices. Zhang et al. used a series of micro-nanofabrication processes to construct p-ZnSe nanowire/n-Si substrate heterojunction [44]. The heterojunction construction follows these steps: photolithography and wet etching with buffered oxide etch (BOE) solution was performed to define the SiO_2 insulating pads on a SiO_2 (300 nm)/n-Si substrate. Then p-ZnSe nanowires were transferred from the growth substrate onto the patterned SiO_2/Si substrate via a simple sliding transfer process. After dispersion, some NWs would cross on the edges of the SiO_2 pads and partially contact with the underlying n-Si substrate. The p-ZnSe nanowire/n-Si heterojunction could be formed in the contact regions. Finally, Au (50 nm) were deposited on the SiO_2 by electron-beam evaporation and served as the ohmic contacts to the NWs. The stepwise process for the construction of the ZnSe nanowire/Si heterojunction is shown in the Figure 8. Many other heterojunctions were fabricated based on the above constructions method, such as ZnSe nanoribbon/Si nano-heterojunction [45], CdS:Ga nanoribbon/Si heterojunctions [46], n-CdSe nanowire/p+-Si substrate heterojunction [47], p-ZnS nanoribbon/n-Si heterojunction [48], p-CdS nanoribbon/n-Si heterojunctions [49], n-CdS nanowire/p+-Si substrate hybrid p-n junction [50],

ZnSe nanowire array/Si p-n heterojunctions [51], ZnSe nanowire/Si p-n heterojunctions [52], and so on. Furthermore, Xie et al. firstly used a Ag-assisted chemical etching method to obtain patterned SiNWs array at particular area on the silicon substrate (Figure 9a). Then, they used mechanically transferred method to transfer CdTe nanoribbons onto the Si substrate and heterojunctions could be formed at the regions where the bottom surface on the nanoribbons contacts with the tips of n-type SiNWs array [53]. Qin et al. fabricated n-CdS$_X$Se$_{1-X}$/p$^+$-Si parallel-nanobelt heterojunctions on a silicon-on-insulator (SOI) substrate [54]. First, the CdS$_X$Se$_{1-X}$ nanoribbon suspension was dropped onto the SOI substrate. Then photoresist pads were patterned by UV lithography on the SOI substrate, with at least one pad covering one end of a single CdS$_X$Se$_{1-X}$ nanoribbon. The photoresist together with the uncovered CdS$_X$Se$_{1-X}$ nanoribbon was then used as the mask for the following Si etching process by an inductively-coupled plasma (ICP) etching technique. Later, the remaining photoresist was removed by acetone. Finally, by UV lithography followed by a thermal evaporation and lift-off process, an In/Au ohmic contact electrode was made on the nanoribbon. The fabrication process is shown in Figure 9b. The constructed n-CdS$_X$Se$_{1-X}$/p$^+$-Si parallel-nanobelts heterojunction was considered to have the advantages of larger active region, smaller series resistance, higher electron and hole injective current. Lee et al. also used SOI substrate to construct a kind of n-CdSe:In nanowire/p-Si nanoribbon crossbar heterojunction which showed high stability and reproducibility in performance [18].
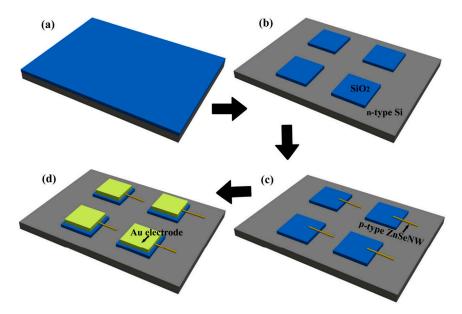

Figure 8. Schematic illustration of the fabrication process of ZnSeNW/Si p-n junction. Reproduced with permission from [44], Copyright 2016, Elsevier B.V.

Yu et al. fabricated n-ZnO nanowire/p-GaN film heterojunctions which were used as UV light-emitting diodes and self-powered UV detector. Mg-doped p-GaN film was first grown by low-temperature metal-organic chemical vapor deposition. A layer of Al$_2$O$_3$ insulating film was then deposited via electron beam heating evaporation onto half of the GaN film using a shadow mask. A single ZnO nanowire was subsequently placed across the boundary between the Al$_2$O$_3$ and GaN films. The natural atomic bonding between the ZnO and GaN formed the p-n heterojunction. Finally, metal electrodes were deposited in order to complete the device fabrication [55,56].
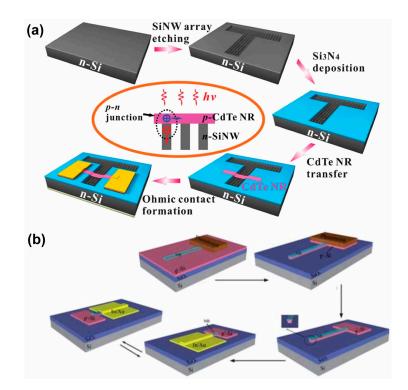
Figure 9. (**a**) Schematic illustration of the fabrication process for the p-CdTeNR/n-SiNW array heterojunction device. Reproduced with permission from [53], Copyright 2012, The Royal Society of Chemistry. (**b**) Flowchart for the fabrication process of the n-CdS$_X$Se$_{1-X}$/p$^+$-Si parallel-nanobelt heterojunctions: (1) The NB suspension was dropped onto the SOI substrate and photoresist pads (200 mm long, 50 mm wide) were patterned by UV lithography. (2) The Si was etched by ICP etching. The photoresist together with the nanobelts were used as the mask. (3) The photoresist was removed. The cross-section at the end of the nanobelts was magnified to show the undercut effect. (4) The final device from two angles of view after the In/Au (10 nm/100 nm) ohmic contact electrode was made. Reproduced with permission from [54], Copyright 2010, The Royal Society of Chemistry.

3. Optoelectronic Applications of Heterojunctions Based on II-VI Compound Semiconductor 1-D Nanostructures

There are many studies on the optoelectronic applications of heterojunctions based on II-VI semiconductor nanostructures, such as solar cells, photodetectors, light emitting diodes, etc. In this section, we mainly focus on the optoelectronic applications of the different types of heterojunctions based on II-VI semiconductor nanostructures. The authors considered that the efficiency was significantly underestimated because the nanowire is relatively thin and the light absorption is far from complete. Furthermore, the efficiency could be increased by surface passivation in order to suppress the carrier recombination of these surface states.

3.1. Solar Cells

Most of II-VI group semiconductors have direct band gaps and high optical absorption and emission coefficients [57]. On the other hand, by combining semiconductors with different band gaps, each part of the heterojunctions can selectively absorb the sunlight in a certain spectrum range, thus leading to wider light absorption and more efficient light utilization. Thereby heterojunctions have shown the great promise for realizing high performance solar cells [39]. A leading candidate for photovoltaic applications is CdTe, which has a band gap of 1.45 eV and high optical absorption coefficient. A film of CdTe with thickness of 2 mm will absorb nearly 100% of incident solar radiation [58]. The most common solar cell configuration is p-CdTe/n-CdS heterojunction. For instance,

Britt et al. successfully demonstrated the fabrication of 1 cm^2 large thin-film CdS/CdTe solar cells with an impressive efficiency of 15.8% under AM 1.5 G illumination [59].

　　In recent years, the studies of solar cells based on II-VI semiconductor nanostructures have caught the eyes of investigators all over the world and gained fruitful results. Yang et al. fabricated a kind of CdS/Cu$_2$S core-shell nanowire solar cells with open-circuit voltage and fill factor values superior to those reported for equivalent planar cells, and an energy conversion efficiency of ~5.4%, which is comparable to that of equivalent planar cells despite low light absorption levels [9,60]. They also integrated multiple cells on single nanowires in both series and parallel configurations for high output voltages and currents (Figure 10). The dramatic photovoltaic performance of CdS/Cu$_2$S core-shell nanowire solar cells is considered to arise from the low-temperature solution-based cation exchange reaction which could create a heterooepitaxial junction between a single-crystalline CdS core and single-crystalline Cu$_2$S shell. Zhou et al. fabricated a kind of photovoltaic device based on a single CdSe/ZnTe core-shell nanowire [55]. In their device, indium and nickel were selected as the electrode materials for the CdSe core and ZnTe shell, respectively. As a result, the device's dark I-V curve exhibits clear rectifying behavior while the rectifying curve shifts downwards due to the generation of photocurrent under illumination. The best CdSe/ZnTe core-shell nanowire solar cell exhibited an open circuit voltage of 0.18 V, a short-circuit current of 38 pA, and a fill factor of 0.38, which yielded an energy conversion efficiency of 1.7%. Zhang et al. also designed photovoltaic devices based on the coaxial ZnSe/ZnO p-n junction [52]. A power conversion efficiency of 1.24% and a large open circuit voltage of 0.87 V under UV light were obtained. The large bandgaps of ZnSe and ZnO and the high quality of the ZnSe/ZnO interface were considered to be related to the high performance of the nano-heterojunction. Zhang et al. developed a kind of ZnO/ZnSe type II core-shell nanowire array solar cell, which could offer strong enhancement in light absorption through increasing the junction area and light trapping. Their result opened up new options in the selecting the absorber material for solar cells [61].
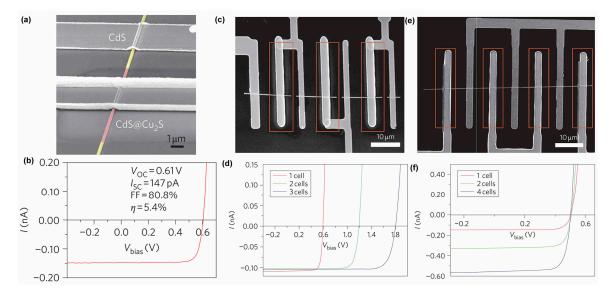

Figure 10. (**a**) SEM image of a PV unit; CdS and Cu$_2$S are highlighted with yellow and brown false colours, respectively. (**b**) I-V characteristic of a core-shell nanowire under 1 sun (AM 1.5 G) illumination. (**c**) SEM image of three PV units from a single nanowire in series with the core-shell regions marked by the brown rectangles. (**d**) I-V characteristic of the in series units under 1 sun illumination (AM 1.5 G), showing that the voltages add and the current remains fixed. (**e**) SEM image of four PV units from a single nanowire in parallel with the core-shell regions marked by the brown rectangles. (**f**) I-V characteristic of the four units in parallel under 1 sun illumination (AM 1.5 G), showing that the currents add and the voltage remains fixed. Reproduced with permission from [9], Copyright 2011, Nature Publishing Group.

Heterojunctions based on II-VI group semiconductor one-dimensional nanostructures and Si substrates were also considered as an important candidate for next-generation solar cells. Wu et al. constructed photovoltaic devices on the basis of the CdS:Ga nanoribbons/Si heterojunctions [46]. The devices presented an obvious PV behavior under AM 1.5 G light illumination: the open circuit photo voltage and the short circuit current are deduced to be 0.45 V and 3.49 nA, respectively, leading to a fill factor of 44.1% and a power conversion efficiency of 1.24%. Considering the large difference in band gap, the CdS:Ga nanoribbon will absorb light with short wavelength, while Si can absorb long wavelength light. The distinct structure of the heterojunction made the incident light with a wide spectrum be absorbed and utilized more efficiently. This feature is superior to those of the conventional solar cells based on Si, which showed poorer absorption in the short wavelength range. Moreover, ZnSe nanowire/Si p-n junction [44], p-ZnSe nanowire array/Si p-n heterojunctions [51], and single ZnSe nanowire/Si p-n heterojunction [52] were achieved based on the configuration of one-dimensional nanostructures and Si substrates, and presented conversion efficiency of ~2.87%, 1.04%, and 1.8%, respectively. To improve the devices' performance, Wang et al. modified Ag nanoparticles on the ZnSe nanoribbon/Si p-n heterojunction and made the photovoltaic performance improve dramatically compared to the device without a Ag nanoparticle, as shown in Figure 11 [45]. It is considered that the enhanced light absorption and electric field strength of the ZnSe nanoribbons modified with Ag nanoparticles by localized surface plasmon resonance could lead to more electron-hole pairs generation and improve the conversion efficiency. On the other hand, Xie and Zhang et al. constructed heterojunctions based on II-VI group semiconductor one-dimensional nanostructures and Si nanowire arrays in order to enhance the light absorption compared to planner Si substrates [39,53]. As a result, a p-CdTeNR/n-SiNW array heterojunction device with a conversion efficiency of 2.1% and a p-ZnSeNRs/CH$_3$-SiNW array heterojunction with a conversion efficiency of 2.27% were obtained.
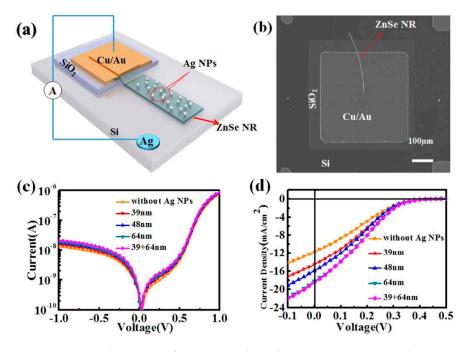

Figure 11. (**a**) Schematic illustration of ZnSe nanoribbon/Si heterojunction. (**b**) The top view SEM image of a single nanoribbon device. (**c**) Dark I-V characteristics of devices in the semi-logarithmic scale. (**d**) The J-V curves of devices embellished with different diameters of Ag nanoparticles measured under AM 1.5 G illumination at 100 mW cm^{-2}. Reproduced with permission from [45], Copyright 2016, IOP Publishing Ltd.

3.2. Photodetectors

II-VI group semiconductors have direct band gaps from 1.5 eV (CdTe) to 3.7 eV (ZnS), and the band gaps of II-VI nanostructures could be further extended via quantum confinement effects. Therefore II-VI nanostructures are very promising candidates for photodetection applications from NIR to UV light. Moreover, photodetectors based on II-VI nanostructures are expected to have much improved performance owing to their high quantum efficiency and high crystal quality [13]. On the other hand, it is worth emphasizing that effective and rapid separation of the photo-generated carriers at heterojunction photodetectors' space-charge region could result in quickly photoresponse, which is very different from the slow time photoconductive relaxation of one-dimensional photoconductors originating from adsorbates on the nanostructures surface [62].

Xie et al. developed a kind of high-performance zero-power photodetector based on a p-CdTeNR/n-SiNWs array heterojunction, which could be operated in the visible to near-infrared range with good stability, high sensitivity, and fast response speed [53]. The photodetectors were run under white light illumination with an intensity of 62.5 μW cm^{-2} and presented excellent stability and reproducibility even at 600 Hz. On the other hand, the heterojunction devices reveals small rise time (1.2 ms) and fall time (1.58 ms), which are much faster than the reported CdTe nanowires and CdTe nanoribbons based photodetectors [63–65]. Wu et al. fabricated CdS nanoribbon/Si heterojunctions based photodiodes and obtained smaller rise time of 300 μs and fall time of 740 μs under white light illumination with intensity of 5.3 mW cm^{-2} (Figure 12) [61]. They think the fast photoresponse of the heterojunction could be attribute to the high-quality p-n junction formed between the CdS nanoribbon and the Si substrate. The interface defects are few, so the photogenerated carriers could be quickly separated by the space charge region and then transferred to the electrodes. Additionally, based on the high-quality ZnS NRs and achievement on ohmic contact, Yu et al. constructed a kind of photodiodes by p-ZnS nanoribbon and n-Si substrate with a response speed as high as ~48 ms (rise time). Furthermore, the device also exhibits stable optoelectrical properties with high sensitivity to UV-VIS-NIR light and an enhancement of responsivities of 1.1×10^3 AW^{-1} for 254 nm under a reverse bias of 0.5 V [48]. Bie et al. prepared self-powered ZnO/GaN nanoscale p-n junctions photodetector with fast response time (219 μs) [55]. It should be pointed out that the nanoscale p-n junction shows visible-blind sharp UV response which is benefitted from the high-quality ZnO and GaN materials and the nanoscale device feature. On the other hand, Wang et al. fabricated ZnSe nanoribbon/Si p-n heterojunction photodetector [45]. To improve its performance, Ag nanoparticles were modified onto the ZnSe nanoribbon/Si p-n heterojunction device (Figure 13). The responsivity and detectivity were improved to 184.8 mAW^{-1} and 9.20×10^{11} cm Hz$^{1/2}$ W^{-1} for device decorated with Ag nanoparticles of 39 + 64 nm compared to 117.2 mAW^{-1} and 5.86×10^{11} cm Hz$^{1/2}$ W^{-1} for device without Ag nanoparticles. When the heterojunction was irradiated by light illumination, the energetic hot electrons from the localized surface plasmon resonance excitation of metallic plasmonic nanoparticles can easily transfer to the nearby ZnSe nanoribbon with a relatively high energy. The injected electrons at the ZnSe nanoribbons could migrate to the ZnSe/Si heterojunction interface, and were then separated by the built-in electric field. Consequently, the plasmonic device exhibits enhanced photocurrent in comparison with a device without Ag nanoparticles.
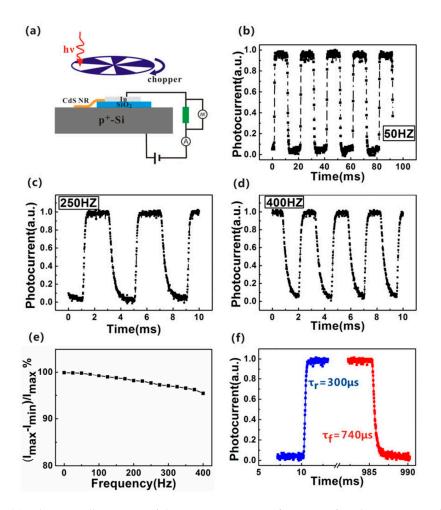
Figure 12. (**a**) Schematic illustration of the measurement configuration for photoresponse detection. Photoresponse characteristics of the CdSNR/Si heterojunction for pulsed light irradiation at frequencies of: (**b**) 50 Hz; (**c**) 250 Hz; and (**d**) 400 Hz. (**e**) The relative balance ($\frac{I_{max}-I_{min}}{I_{max}}$) versus the switching frequency. (**f**) Enlarged rising and falling edges for calculating the rise and fall times. Reproduced with permission from [46], Copyright 2011, IOP Publishing Ltd.
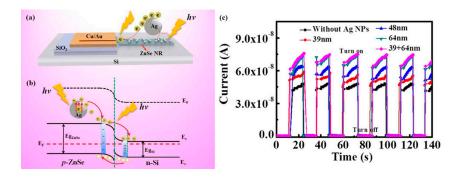

Figure 13. (**a**) Schematic illustration of the localized surface plasmon resonance excited electrons transfer from Ag nano particles to ZnSe nanoribbon. (**b**) Energy band diagram of ZnSe nanoribbon/Si heterojunction modified with Ag nanoparticles under light illumination. (**c**) Time response spectra of the devices without and with decoration of 39, 48, 64, and 39 + 64 nm Ag nanoparticles measured at zero voltage bias. Reproduced with permission from [45], Copyright 2016, IOP Publishing Ltd.

Luo et al. constructed CdS-ZnTe core-shell nano-heterojunction photodetectors and measured their photoresponse under light illumination with a wavelength of 638 nm and light intensity of 2 mW cm^{-2} at 1 V (Figure 14) [25]. The fabricated core-shell nano-heterojunction photodetectors

exhibited responsivity of 1.55×10^3 AW^{-1}, conductive gain of 3.3×10^3, detectivity of 8.7×10^{12} cm Hz$^{1/2}$ W^{-1}, which are much higher than the devices based on is greatly enhanced by the piezo-phototronic effect [34]. Jie et al. fabricated Ge-CdS core-shell heterojunction nanowire photodetectors with excellent diode characteristics and a pronounced photoresponse under light illumination. Significantly, owing to the existence of a built-in electric field, the heterojunctions could serve as self-driven photodetectors, with a high photodetection sensitivity of 18,000%, which is remarkably much higher than arrays of CdS nanowires and CdS quantum dots [65,66]. Zhou et al. also prepared a broad band photodetector based on II-VI binary CdSe/ZnTe core/shell nanowire array. Its photodetection is better than previous reports on Ge nanowire photodetectors. The complementary bandgaps of Ge and CdS also ensured that the device had a capability for broadband detection from visible to infrared light. This study represents an important advance in fabricating core-shell heterojunction NWs for high-performance optoelectronic applications [29]. Wang et al. developed an efficient and highly sensitive broad band UV/VIS photodetector based on wide band gap ZnO/ZnS heterojunction 3D core/shell nanowire array [37]. The abrupt interface between ZnO and ZnS plays a dominant role in photon absorption via an indirect type-II transition which was strongly manifested in the photodetection of visible illumination (blue and green). The absolute device responsivity was further increased through the piezo-phototronic effect by an order of magnitude under simultaneous application of load and illumination, resulting in three orders of change in the relative responsivity. Moreover, photodetectors based on a crossed ZnSe-ZnO p-n nano-heterojunction and ZnSe-ZnO axial p-n junction were constructed and exhibited excellent diode behaviors and heigh sensitivity to ultraviolet light ilumination with good reproducibility and quick photoresponse [39,43]. Both devices showed much higher performance than the photodetectors based on ZnO, ZnTe, and CdSe nanowires [67–69].
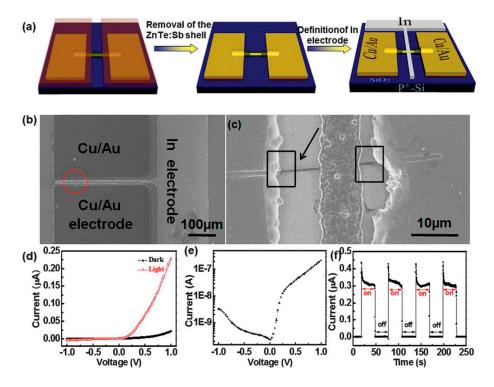

Figure 14. (**a**) Stepwise process for the fabrication of a single CdS:Ga-ZnTe:Sb nanostructures. (**b**,**c**) Representative FESEM images of a p-n junction device. (**d**) Rectification characteristics of the p-n junction measured both in the dark and under light illumination. (**e**) I-V curve of the p-n junction under light illumination at a log scale. (**f**) Photoresponse of the CdS:Ga-ZnTe:Sb nanostructures to the pulsed light illumination, and the bias voltage is 1 V. Reproduced with permission from [29], Copyright 2011, The Royal Society of Chemistry.

3.3. Other Applications

There are many other electronic and optoelectronic applications for heterojunctions based on II-VI group semiconductors, such as light emitting diodes, junction field-effect transistors, avalanche photodiodes, etc. [18,41,42,47,50,53,54]. He and his co-workers firstly constructed a type of CdSe/Si nano-heterojunction and then utilized the p-Si nanoribbons as gates and n-CdSe nanowires as conduction channels to act as the nano-heterojunction junction field-effect transistors with high stability and reproducibility in performance [18]. The electrical characteristics were shown in Figure 15. It should be noted that the subthreshold swing value of this device (67 mV/dec) is only one-ninth of the best values obtained from the top-gate devices and is very close to the theoretical limit (60 mV/dec). On the other hand, the conductance of the device can be tuned by a factor of near 10^3 by a small gate voltage variation from -2 to -1 V, concerning the nanoscale diameter of CdSe nanowires, the channel width and thus source-drain current can be sensitively manipulated by the reverse gate bias. Moreover, Lieber and cooperators firstly developed nanoscale avalanche photodiodes from crossed p-Si and n-type CdS nanowire diodes (Figure 16) [41]. Their studies presented that the nanoscale avalanche photodiodes exhibit ultrahigh sensitivity with detection limits of less than 100 photons, a subwavelength spatial resolution of at least 250 nm, excellent polarization sensitivity, and can be assembled into small arrays. This excellent performance offers substantial promise in diverse areas ranging from nanopositioning, integrated photonics, and near-field detection to real-time observation of single dynamics.
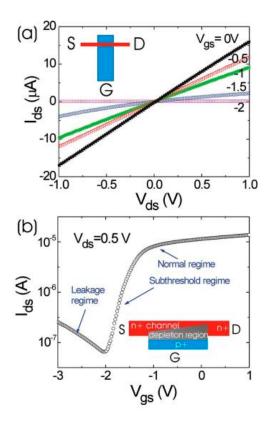

Figure 15. (**a**) Gate voltage-dependent I_{ds}-V_{ds} characteristics of a crossbar junction field effect transistor. The inset shows the schematic diagram of the crossbar junction field effect transistor constructed with Si nanoribbon as a gate and CdSe nanowire as a source-drain channel. (**b**) I_g-V_{gs} curve measured at $V_{ds} = 0.5$ V. A depletion layer with its thickness controlled by V_{gs} is formed at the Si nanoribbon and CdSe nanowire interface, as depicted in the inset. Reproduced with permission from [18], Copyright 2009, American Institute of Physics.
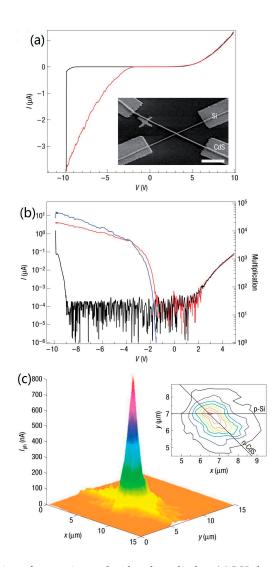
Figure 16. Characterization of nanowire avalanche photodiodes. (**a**) I-V characteristic of the avalanche photodiodes in dark (black line) and illuminated (red line) conditions; the device was illuminated with 500 nW of 488-nm light (red line). The inset shows a scanning electron micrograph of the n-CdS/p-Si device; the scale bar is 4 μm. (**b**) Logarithmic scale of avalanche photodiodes I-V characteristics (black line: dark; red line: illuminated) and the corresponding multiplication factor (blue line). (**c**) Plot of the spatially-resolved photocurrent from the nano-avalanche photodiodes measured in the proportional mode using a diffraction-limited laser; the bias voltage, laser power and scanning step size were −7 V, 200 nW, and 250 nm (in *x* and *y*), respectively. The inset shows a contour plot with slices taken every 100 nA. The nanowire positions are indicated on the plot by solid lines. Reproduced with permission from [44], Copyright 2006, Nature Publishing Group.

In recent years, many semiconductor one-dimensional light emitting diodes have been studied. Qin et al. used the n-type CdS_XSe_{1-X} alloy nanobelts and p-type Si nanobelts as building blocks to construct novel high efficiency color tunable parallel-nanobelts heterojunction light emitting diodes [54]. The device structure has the advantage of larger active region, smaller series resistance, higher electron and hole injective current, and lower turn-on voltage. Figure 17 shows the room temperature EL spectra for several representative $n\text{-}CdS_XSe_{1-X}$/Si parallel-nanobelt heterojunction light emitting diodes at various forward biases from 2 to 7 V. The x value changes from 1 to 0. Consequently, the device emitted strong EL light spot from red to green (510–708 nm) which could be taken by a camera. This device configuration was considered to promise a bright future in various nano-device applications, such as electrically-driven lasers, multi-color displays,

white light illumination, etc. Lieber and his co-workers demonstrated the assembly of a wide range of efficient direct-gap II-VI and III-VI semiconductor nanowires with silicon nanowires and planar silicon structures to produce multicolor, electrically-driven nanophotonic and integrated nanoelectronic-photonic systems [42]. Figure 18 depicts the electroluminescence of spectra from crossed p-n diodes of p-Si and n-CdS, CdSSe, CdSe, and InP, which shows an EL peak maxima and images characteristic of band-edge emission from the crossed junctions made with these materials: $CdS_{0.5}Se_{0.5}$, 600 nm; CdSe, 700 nm; and InP, 820 nm. Furthermore, the authors developed the ability to form nano-LEDs with non-emissive Si nanowire hole-injectors to assemble multicolor arrays consisting of n-type GaN, CdS, and CdSe nanowires crossing a single p-type Si nanowire. Normalized emission spectra recorded from the array demonstrated three spatially- and spectrally-distinct peaks with maxima at 365, 510, and 690 nm consistent with band-edge emission from GaN, CdS, and CdSe, respectively. In addition, color images of electroluminescence from the array shows the green and red emission from p-Si/n-CdS and p-Si/n-CdSe crosses, respectively. The ability to assemble different materials and independently tune the emission from each nano-LED offers substantial potential producing specific wavelength sources, and demonstrates an important step towards integrated nanoscale photonic circuits.
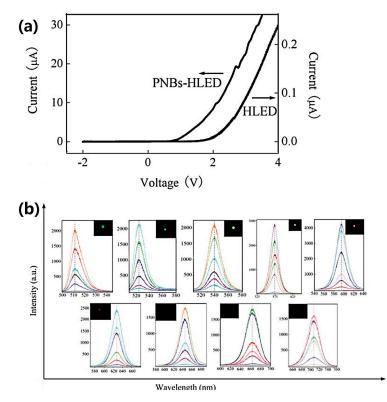
Figure 17. (**a**) Typical I-V curves of a parallel-nanobelts heterojunction light emitting diodes and a heterojunction light emitting diodes with point-shaped active region. The turn-on voltages for them are 0.5 and 1.8 V, respectively. (**b**) Room-temperature EL spectra of the $n\text{-}CdS_XSe_{1-X}/p^+\text{-}Si$ parallel-nanobelts heterojunction light emitting diodes with the x value changing from 1 to 0 at the forward biases of 2–7 V, together with the corresponding visible light spots at 7 V. Reproduced with permission from [54], Copyright 2010, The Royal Society of Chemistry.
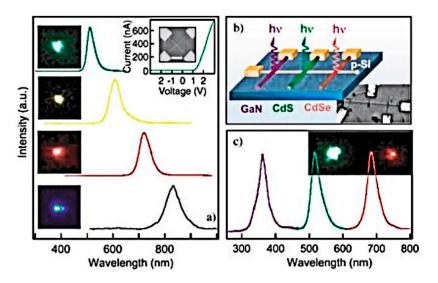
Figure 18. (**a**) EL spectra from crossed p-n diodes of p-type Si and n-type CdS, CdSSe, CdSe, and InP, respectively (top to bottom). Insets to the left are the corresponding EL images for CdS, CdSSe, CdSe (all color CCD), and InP (liquid-nitrogen-cooled CCD) nanoLEDs. The inset top right shows representative I-V and SEM data recorded for a p-Si/n-CdS crossed nanowire junction (scale bar = 1 mm); spectra and images were collected at +5 V).; (**b**) schematic and corresponding SEM image of a tricolor nanoLED array. The array was obtained by fluidic assembly and photolithography with 5 mm separation between NW emitters. (**c**) Normalized EL spectra and color images from the three elements. Reproduced with permission from [53], Copyright 2005, Wiley-VCH.

4. Conclusions and Outlook

In this review, we comprehensively discussed the significant progresses in construction and optoelectronic applications of heterojunctions based on II-VI compound semiconductor one-dimensional nanostructures in the past decade. Various construction strategies toward different types of heterojunctions were studied by researchers, including core-shell heterojunctions, one-dimensional axial heterojunctions, crossed nanowires heterojunctions, and one-dimensional nanostructure/thin film or Si substrate heterojunctions. Additionally, optoelectronic applications of these constructed heterojunctions, such as photodetectors, solar cells, light emitting diodes, and junction field effect transistors have been discussed and showed superior performance to those made of their film counterparts. This review shows that heterojunctions based on II-VI compound semiconductor 1-D nanostructures have great potential for future optoelectronic applications. On the other hand, although many significant achievements have been made in the construction and optoelectronic applications of heterojunctions based on II-VI compound semiconductor one-dimensional nanostructures, further efforts are required to solve problems, such as controllable fabrication with high uniformity and alignment, development of heterojunction architectures, integration of optoelectronic devices based on heterojunctions at the large scale for practical applications, and the development of flexible optoelectronic devices appropriate for wearable devices. With the nanotechnology improving, we believe that these problems will be solved and heterojunctions based on II-VI compound semiconductor 1-D nanostructures will exhibit great potential on the next-generation of scaled down, flexible, low-power electronics and optoelectronics.

Author Contributions: Xiwei Zhang wrote this paper; and Di Wu and Huijuan Geng worked on the revision of the final version of manuscript.

Conflicts of Interest: The authors declare no conflict of interest.

References

1. Chuang, S.; Gao, Q.; Kapadia, R.; Ford, A.C.; Guo, J.; Javey, A. Ballistic InAs nanowire transistors. *Nano Lett.* **2013**, *13*, 555–558. [CrossRef] [PubMed]

2. Hochbaum, A.I.; Yang, P. Semiconductor nanowires for energy conversion. *Chem. Rev.* **2009**, *110*, 527–546. [CrossRef] [PubMed]

3. Mao, J.; Ding, K.; Jie, J. The way to high-performance single nanowire photodetectors: Problems and prospects. *Sci. China Phys. Mech.* **2016**, *60*, 017031. [CrossRef]

4. Zhai, T.; Li, L.; Wang, X.; Fang, X.; Bando, Y.; Golberg, D. Recent Developments in One-Dimensional Inorganic Nanostructures for Photodetectors. *Adv. Funct. Mater.* **2010**, *20*, 4233–4248. [CrossRef]

5. Zhang, Q.; Liu, H.; Guo, P.; Li, D.; Fan, P.; Zheng, W.; Zhu, X.; Jiang, Y.; Zhou, H.; Hu, W.; et al. Vapor growth and interfacial carrier dynamics of high-quality CdS-CdSSe-CdS axial nanowire heterostructures. *Nano Energy* **2017**, *32*, 28–35. [CrossRef]

6. Wu, D.; Jiang, Y.; Wang, L.; Li, S.; Wu, B.; Lan, X.; Yu, Y.; Wu, C.; Wang, Z.; Jie, J. High-performance CdS: P nanoribbon field-effect transistors constructed with high-κ dielectric and top-gate geometry. *Appl. Phys. Lett.* **2010**, *96*, 123118. [CrossRef]

7. Lou, Z.; Li, L.; Shen, G. Ultraviolet/visible photodetectors with ultrafast, high photosensitivity based on 1D ZnS/CdS heterostructures. *Nanoscale* **2016**, *8*, 5219–5225. [CrossRef] [PubMed]

8. Guo, X.; Ying, Y.; Tong, L. Photonic nanowires: From subwavelength waveguides to optical sensors. *Acc. Chem. Res.* **2013**, *47*, 656–666. [CrossRef] [PubMed]

9. Zhang, X.; Mao, J.; Shao, Z.; Diao, S.; Hu, D.; Tang, Z.; Wu, H.; Jie, J. Efficient photovoltaic devices based on p-ZnSe/n-CdS core–shell heterojunctions with high open-circuit voltage. *J. Mater. Chem. C* **2017**, *5*, 2107–2113. [CrossRef]

10. Haberern, K.W.; Baude, P.F.; Flamholtz, S.J.; Buijs, M.; Horikx, J.J.L.; Law, K.K.; Haase, M.A.; Miller, T.J.; Haugen, G.M. II-VI index-guided lasers for optical recording. In *In-Plane Semiconductor Lasers: From Ultraviolet to Midinfrared*; SPIE: Bellingham, WA, USA, 1997; Volume 3001, pp. 101–105.

11. Green, M.A. Third-generation Photovoltaics: Advanced Solar Energy Conversion. *Phys. Today* **2004**, *57*, 71–72.

12. Schlesinger, T.E.; James, R.B. *Semiconductors for Room Temperature Nuclear Applications*; Academic Press: Cambridge, MA, USA, 1995; Volume 43, p. 335.

13. Jie, J.; Zhang, W.; Bello, I.; Lee, S.-T. One-dimensional II-VI nanostructures: Synthesis, properties and optoelectronic applications. *Nano Today* **2010**, *5*, 313–336. [CrossRef]

14. Liu, Y.; Zapien, J.A.; Shan, Y.Y.; Geng, C.-Y.; Lee, C.S.; Lee, S.-T. Wavelength-controlled lasing in $Zn_XCd_{1−X}S$ single-crystal nanoribbons. *Adv. Mater.* **2005**, *17*, 1372–1377. [CrossRef]

15. Hu, L.; Yan, J.; Kim, Y.; Fei, G.; Watanabe, K.; Sekiguchi, T.; Zhang, L.; Fang, X. Cathodoluminescence and photoconductive characteristics of single-crystal ternary CdS/CdSe/CdS biaxial nanobelts. *Small* **2015**, *11*, 1531–1536. [CrossRef] [PubMed]

16. Zhang, Y.; Dong, H.; Tang, Q.; Ferdous, S.; Liu, F.; Mannsfeld, S.C.B.; Hu, W.; Briseno, A.L. Organic single-crystalline p-n junction nanoribbons. *J. Am. Chem. Soc.* **2010**, *132*, 11580–11584. [CrossRef] [PubMed]

17. Tian, B.; Kempa, T.J.; Lieber, C.M. Single nanowire photovoltaics. *Chem. Soc. Rev.* **2009**, *38*, 16–24. [CrossRef] [PubMed]

18. He, Z.B.; Zhang, W.J.; Tang, Y.B.; Wang, H.B.; Cao, Y.L.; Song, H.S.; Bello, I.; Lee, C.S.; Lee, S.T. Crossbar heterojunction field effect transistors of CdSe: In nanowires and Si nanoribbons. *Appl. Phys. Lett.* **2009**, *95*, 253107. [CrossRef]

19. Wang, D.; Qian, F.; Yang, C.; Zhong, Z.; Lieber, C.M. Rational growth of branched and hyperbranched nanowire structures. *Nano Lett.* **2004**, *4*, 871–874. [CrossRef]

20. Jeon, P.J.; Lee, Y.T.; Lim, J.Y.; Kim, J.S.; Hwang, D.K.; Im, S. Black Phosphorus-Zinc Oxide Nanomaterial Heterojunction for p-n Diode and Junction Field-Effect Transistor. *Nano Lett.* **2016**, *16*, 1293–1298. [CrossRef] [PubMed]

21. Wu, C.; Jie, J.; Wang, L.; Yu, Y.; Peng, Q.; Zhang, X.; Cai, J.; Guo, H.; Wu, D.; Jiang, Y. Chlorine-doped n-type CdS nanowires with enhanced photoconductivity. *Nanotechnology* **2010**, *21*, 505203. [CrossRef] [PubMed]

22. Duan, X.; Huang, Y.; Agarwal, R.; Lieber, C.M. Single-nanowire electrically driven lasers. *Nature* **2003**, *421*, 241. [CrossRef] [PubMed]

23. Huang, Y.Y.; Chen, L.Y.; Chang, C.H.; Sun, Y.H.; Cheng, Y.W.; Ke, M.Y.; Lu, Y.H.; Kuo, H.C.; Huang, J. Investigation of low-temperature electroluminescence of InGaN/GaN based nanorod light emitting arrays. *Nanotechnology* **2010**, *22*, 045202. [CrossRef] [PubMed]

24. Kempa, T.J.; Tian, B.; Kim, D.R.; Hu, J.; Zheng, X.; Lieber, C.M. Single and tandem axial pin nanowire photovoltaic devices. *Nano Lett.* **2008**, *8*, 3456–3460. [CrossRef] [PubMed]

25. Wang, L.; Song, H.W.; Liu, Z.X.; Ma, X.; Chen, R.; Yu, Y.Q.; Wu, C.Y.; Hu, J.G.; Zhang, Y.; Li, Q.; et al. Core–shell CdS: Ga-ZnTe:Sb p-n nano-heterojunctions: Fabrication and optoelectronic characteristics. *J. Mater. Chem. C* **2015**, *3*, 2933–2939. [CrossRef]

26. Wang, K.; Rai, S.C.; Marmon, J.; Chen, J.; Yao, K.; Wozny, S.; Cao, B.; Yan, Y.; Zhang, Y.; Zhou, W. Nearly lattice matched all wurtzite CdSe/ZnTe type II core–shell nanowires with epitaxial interfaces for photovoltaics. *Nanoscale* **2014**, *6*, 3679–3685. [CrossRef] [PubMed]

27. Tang, J.; Huo, Z.; Brittman, S.; Cao, H.; Yang, P. Solution-processed core–shell nanowires for efficient photovoltaic cells. *Nat. Nanotechnol.* **2011**, *6*, 568–572. [CrossRef] [PubMed]

28. Zhang, X.; Meng, D.; Hu, D.; Tang, Z.; Niu, X.; Yu, F.; Ju, L. Construction of coaxial ZnSe/ZnO p-n junctions and their photovoltaic applications. *Appl. Phys. Express* **2016**, *9*, 025201. [CrossRef]

29. Sun, Z.; Shao, Z.; Wu, X.; Jiang, T.; Zheng, N.; Jie, J. High-sensitivity and self-driven photodetectors based on Ge-CdS core–shell heterojunction nanowires via atomic layer deposition. *Cryst. Eng. Comm.* **2016**, *18*, 3919–3924. [CrossRef]

30. Wang, L.; Jie, J.; Wu, C.; Wang, Z.; Yu, Y.; Peng, Q.; Zhang, X.; Hu, Z.; Wu, D.; Guo, H. Coaxial ZnSe/Si nanocables with controlled p-type shell doping. *Nanotechnology* **2010**, *21*, 285206. [CrossRef] [PubMed]

31. Yan, J.; Fang, X.S.; Zhang, L.D.; Bando, Y.; Gautam, U.; Dierre, B.; Sekiguchi, T.; Golberg, D. Structure and Cathodoluminescence of Individual ZnS/ZnO Biaxial Nanobelt Heterostructures. *Nano Lett.* **2008**, *8*, 2794–2799. [CrossRef] [PubMed]

32. Hu, L.; Yan, J.; Liao, M.; Xiang, H.; Gong, X.; Zhang, L.; Fang, X. An optimized ultraviolet-a light photodetector with wide-range photoresponse based on zns/zno biaxial nanobelt. *Adv. Mater.* **2012**, *24*, 2305–2309. [CrossRef] [PubMed]

33. Zhao, B.; Wang, F.; Chen, H.; Wang, Y.; Jiang, M.; Fang, X.; Zhao, D. Solar-blind avalanche photodetector based on single ZnO-Ga$_2$O$_3$ core-shell microwire. *Nano Lett.* **2015**, *15*, 3988–3993. [CrossRef] [PubMed]

34. Rai, S.C.; Wang, K.; Chen, J.; Marmon, J.K.; Bhatt, M.; Wozny, S.; Zhang, Y.; Zhou, W. Enhanced Broad Band Photodetection through Piezo-Phototronic Effect in CdSe/ZnTe Core/Shell Nanowire Array. *Adv. Electron. Mater.* **2015**, *1*, 1400050. [CrossRef]

35. Rai, S.C.; Wang, K.; Ding, Y.; Marmon, J.K.; Bhatt, M.; Zhang, Y.; Zhou, W.; Wang, Z.L. Piezo-phototronic effect enhanced UV/visible photodetector based on fully wide band gap type-II ZnO/ZnS core/shell nanowire array. *ACS Nano* **2015**, *9*, 6419–6427. [CrossRef] [PubMed]

36. Heurlin, M.; Wickert, P.; Fält, S.; Borgström, M.T.; Deppert, K.; Samuelson, L.; Magnusson, M.H. Axial InP nanowire tandem junction grown on a silicon substrate. *Nano Lett.* **2011**, *11*, 2028–2031. [CrossRef] [PubMed]

37. Lysov, A.; Vinaji, S.; Offer, M.; Gutsche, C.; Regolin, I.; Mertin, W.; Geller, M.; Prost, W.; Bacher, G.; Tegude, F.-J. Spatially resolved photoelectric performance of axial GaAs nanowire pn-diodes. *Nano Res.* **2011**, *4*, 987–995. [CrossRef]

38. Zhang, X.; Zhang, X.; Zhang, X.; Zhang, Y.; Bian, L.; Wu, Y.; Xie, C.; Han, Y.; Wang, Y.; Gao, P.; et al. ZnSe nanoribbon/Si nanowire p-n heterojunction arrays and their photovoltaic application with graphene transparent electrodes. *J. Mater. Chem.* **2012**, *22*, 22873–22880. [CrossRef]

39. Zhang, X.; Hu, D.; Tang, Z.; Ma, D. Construction of ZnSe-ZnO axial p-n junctions via regioselective oxidation process and their photo-detection applications. *Appl. Surf. Sci.* **2015**, *357*, 1939–1943. [CrossRef]

40. Huang, Y.; Duan, X.; Wei, Q.; Lieber, C.M. Directed assembly of one-dimensional nanostructures into functional networks. *Science* **2001**, *291*, 630–633. [CrossRef] [PubMed]

41. Hayden, O.; Agarwal, R.; Lieber, C.M. Nanoscale avalanche photodiodes for highly sensitive and spatially resolved photon detection. *Nat. Mater.* **2006**, *5*, 352. [CrossRef] [PubMed]

42. Huang, Y.; Duan, X.; Lieber, C.M. Nanowires for integrated multicolor nanophotonics. *Small* **2005**, *1*, 142–147. [CrossRef] [PubMed]

43. Nie, B.; Luo, L.B.; Chen, J.J.; Hu, J.G.; Wu, C.Y.; Wang, L.; Yu, Y.Q.; Zhu, Z.F.; Jie, J.S. Fabrication of p-type ZnSe: Sb nanowires for high-performance ultraviolet light photodetector application. *Nanotechnology* **2013**, *24*, 095603. [CrossRef] [PubMed]

44. Zhang, X.; Tang, Z.; Hu, D.; Meng, D.; Jia, S. Nanoscale p-n junctions based on p-type ZnSe nanowires and their optoelectronic applications. *Mater. Lett.* **2016**, *168*, 121–124. [CrossRef]

45. Wang, L.; Chen, R.; Ren, Z.F.; Ge, C.W.; Liu, Z.X.; He, S.J.; Yu, Y.Q.; Wu, C.Y.; Luo, L.B. Plasmonic silver nanosphere enhanced ZnSe nanoribbon/Si heterojunction optoelectronic devices. *Nanotechnology* **2016**, *27*, 215202. [CrossRef] [PubMed]

46. Wu, D.; Jiang, Y.; Li, S.; Li, F.; Li, J.; Lan, X.; Zhang, Y.; Wu, C.; Luo, L.; Jie, J. Construction of high-quality CdS: Ga nanoribbon/silicon heterojunctions and their nano-optoelectronic applications. *Nanotechnology* **2011**, *22*, 405201. [CrossRef] [PubMed]

47. Hu, Z.; Zhang, X.; Xie, C.; Wu, C.; Zhang, X.; Bian, L.; Wu, Y.; Wang, L.; Zhang, Y.; Jie, J. Doping dependent crystal structures and optoelectronic properties of n-type CdSe: Ga nanowries. *Nanoscale* **2011**, *3*, 4798–4803. [CrossRef] [PubMed]

48. Yu, Y.Q.; Luo, L.B.; Zhu, Z.F.; Nie, B.; Zhang, Y.G.; Zeng, L.H.; Zhang, Y.; Wu, C.Y.; Wang, L.; Jiang, Y. High-speed ultraviolet-visible-near infrared photodiodes based on p-ZnS nanoribbon-n-silicon heterojunction. *Cryst. Eng. Comm.* **2013**, *15*, 1635–1642. [CrossRef]

49. Xie, C.; Li, F.; Zeng, L.; Luo, L.; Wang, L.; Wu, C.; Jie, J. Surface charge transfer induced p-CdS nanoribbon/n-Si heterojunctions as fast-speed self-driven photodetectors. *J. Mater. Chem. C* **2015**, *3*, 6307–6313. [CrossRef]

50. Cai, J.; Jie, J.; Jiang, P.; Wu, D.; Xie, C.; Wu, C.; Wang, Z.; Yu, Y.; Wang, L.; Zhang, X.; et al. Tuning the electrical transport properties of n-type CdS nanowires via Ga doping and their nano-optoelectronic applications. *Phys. Chem. Chem. Phys.* **2011**, *13*, 14663–14667. [CrossRef] [PubMed]

51. Wang, L.; Lu, M.; Wang, X.; Wu, D.; Xie, C.; Wu, C.; Wang, Z.; Yu, Y.; Wang, L.; Zhang, X.; et al. Tuning the p-type conductivity of ZnSe nanowires via silver doping for rectifying and photovoltaic device applications. *J. Mater. Chem. A* **2013**, *1*, 1148–1154. [CrossRef]

52. Zhang, X.; Zhang, X.; Wang, L.; Wu, Y.; Wang, Y.; Gao, P.; Han, Y.; Jie, J. ZnSe nanowire/Si p-n heterojunctions: Device construction and optoelectronic applications. *Nanotechnology* **2013**, *24*, 395201. [CrossRef] [PubMed]

53. Xie, C.; Luo, L.B.; Zeng, L.H.; Zhu, L.; Chen, J.J.; Nie, B.; Hu, J.G.; Li, Q.; Wu, C.Y.; Wang, L.; et al. p-CdTe nanoribbon/n-silicon nanowires array heterojunctions: Photovoltaic devices and zero-power photodetectors. *Cryst. Eng. Comm.* **2012**, *14*, 7222–7228. [CrossRef]

54. Liu, C.; Dai, L.; Ye, Y.; Sun, T.; Peng, R.G.; Wen, X.; Wu, P.; Qin, G. High-efficiency color tunable n-CdSxSe1−x/p+-Si parallel-nanobelts heterojunction light-emitting diodes. *J. Mater. Chem.* **2010**, *20*, 5011–5015. [CrossRef]

55. Bie, Y.Q.; Liao, Z.M.; Zhang, H.Z.; Li, G.R.; Ye, Y.; Zhou, Y.B.; Xu, J.; Qin, Z.X.; Dai, L.; Yu, D.P. Self-Powered, Ultrafast, Visible-Blind UV Detection and Optical Logical Operation based on ZnO/GaN Nanoscale p-n Junctions. *Adv. Mater.* **2011**, *23*, 649–653. [CrossRef] [PubMed]

56. Bie, Y.Q.; Liao, Z.M.; Wang, P.W.; Zhou, Y.B.; Han, X.B.; Ye, Y.; Zhao, Q.; Wu, X.S.; Dai, L.; Xu, J.; et al. Single ZnO Nanowire/p-type GaN Heterojunctions for Photovoltaic Devices and UV Light-Emitting Diodes. *Adv. Mater.* **2010**, *22*, 4284–4287. [CrossRef] [PubMed]

57. Afzaal, M.; O'Brien, P. Recent developments in II-VI and III-VI semiconductors and their applications in solar cells. *J. Mater. Chem.* **2006**, *16*, 1597–1602. [CrossRef]

58. Ferekides, C.S.; Balasubramanian, U.; Mamazza, R.; Viswanathan, V.; Zhao, H.; Morel, D.L. CdTe thin film solar cells: Device and technology issues. *Sol. Energy* **2004**, *77*, 823–830. [CrossRef]

59. Britt, J.; Ferekides, C. Thin-film CdS/CdTe solar cell with 15.8% efficiency. *Appl. Phys. Lett.* **1993**, *62*, 2851–2852. [CrossRef]

60. Martinuzzi, S. Trends and problems in CdS/CuxS thin film solar cells: A review. *Sol. Cells* **1982**, *5*, 243–268. [CrossRef]

61. Zhou, J.; Gu, Y.; Hu, Y.; Mai, W.; Yeh, P.H.; Bao, G.; Sood, A.K.; Polla, D.L.; Wang, Z.L. Gigantic enhancement in response and reset time of ZnO UV nanosensor by utilizing Schottky contact and surface functionalization. *Appl. Phys. Lett.* **2009**, *94*, 191103. [CrossRef] [PubMed]

62. Kum, M.C.; Jung, H.; Chartuprayoon, N.; Chen, W.; Mulchandani, A.; Myung, N.V. Tuning electrical and optoelectronic properties of single cadmium telluride nanoribbon. *J. Phys. Chem. C* **2012**, *116*, 9202–9208. [CrossRef]

63. Zhang, Y.; Wu, Z.; Zheng, J.; Lin, X.; Zhan, H.; Li, S.; Kang, J.; Bleuse, J.; Mariette, H. ZnO/ZnSe type II core-shell nanowire array solar cell. *Sol. Energy Mater. Sol. C* **2012**, *102*, 15–18. [CrossRef]

64. Ye, Y.; Dai, L.; Sun, T.; You, L.P.; Zhu, R.; Gao, J.Y.; Peng, R.M.; Yu, D.P.; Qin, G.G. High-quality CdTe nanowires: Synthesis, characterization, and application in photoresponse devices. *J. Appl. Phys.* **2010**, *108*, 044301. [CrossRef]

65. Amos, F.F.; Morin, S.A.; Streifer, J.A.; Hamers, R.J.; Jin, S. Photodetector arrays directly assembled onto polymer substrates from aqueous solution. *J. Am. Chem. Soc.* **2007**, *129*, 14296–14302. [CrossRef] [PubMed]

66. He, J.; Chen, J.; Yu, Y.; Zhang, L.; Zhang, G.; Jiang, S.; Liu, W.; Song, H.; Tang, J. Effect of ligand passivation on morphology, optical and photoresponse properties of CdS colloidal quantum dots thin film. *J. Mater. Sci. Mater. Electron.* **2014**, *25*, 1499–1504. [CrossRef]

67. Wu, D.; Jiang, Y.; Zhang, Y.; Li, J.; Yu, Y.; Zhang, Y.; Zhu, Z.; Wang, L.; Wu, C.; Luo, L.; et al. Device structure-dependent field-effect and photoresponse performances of p-type ZnTe: Sb nanoribbons. *J. Mater. Chem.* **2012**, *22*, 6206–6212. [CrossRef]

68. Chang, S.P.; Lu, C.Y.; Chang, S.J.; Chiou, Y.Z.; Hsueh, T.J.; Hsu, C.L. Electrical and optical characteristics of UV photodetector with interlaced ZnO nanowires. *IEEE J. Sel. Top. Quantum* **2011**, *17*, 990–995. [CrossRef]

69. Cao, Y.L.; Liu, Z.T.; Chen, L.M.; Tang, Y.B.; Luo, L.B.; Jie, J.S.; Zhang, W.J.; Lee, S.T.; Lee, C.S. Single-crystalline ZnTe nanowires for application as high-performance Green/Ultraviolet photodetector. *Opt. Express* **2011**, *19*, 6100–6108. [CrossRef] [PubMed]